



Influence of fiber breakage on flow behavior in fiber length- and orientation-dependent injection molding simulations

Florian Wittemann^{a,*}, Luise Kärger^a, Frank Henning^{a,b}

^a Karlsruhe Institute of Technology (KIT), Institute of Vehicle System Technology, Lightweight Technology, Rintheimer Querallee 2, 76131 Karlsruhe, Germany

^b Fraunhofer Institute for Chemical Technology (ICT), Joseph-von-Fraunhofer-Straße 7, 76327 Pfalz, Germany

ARTICLE INFO

Keywords:

Discontinuous fiber reinforced polymers
Injection molding simulation
Anisotropic flow
Hydrodynamic forces
Fiber breakage modeling

ABSTRACT

Injection molding is one of the most important processes for manufacturing discontinuous fiber reinforced polymers (FRPs). The matrix of FRPs shows a transient chemo-thermomechanical behavior and the fibers create anisotropy influencing physical properties. Hence, FRPs are complex materials, but also likely used in volume production. In this work, the fiber-induced anisotropic behavior during mold filling is modelled with an anisotropic fourth order viscosity tensor. The viscosity tensor takes second and fourth order fiber orientation tensor, fiber length and non-Newtonian matrix viscosity into account. In this way, the macroscopic simulation captures the influence of the flow field on the fiber re-orientation and vice versa. The fiber orientation tensor is used to determine reference fibers in every element for calculation of hydrodynamic forces. This information is used in a novel fiber breakage model, based on buckling of fibers in Jeffery's orbit. The result is a macroscopic molding simulation with not only transient fiber orientation distribution, but also fiber length distribution. Due to the anisotropic viscosity tensor, the predicted fiber breakage influences the material's viscosity and flow behavior, which is also visible in the simulated cavity pressure. The results are validated with injection molding experiments, performed with a glass fiber reinforced phenolic compound, showing good agreement.

1. Introduction

Today's injection molded parts are often made with discontinuous fiber reinforced polymers (FRPs), especially if the mechanical properties are important. The presence of fibers causes anisotropic material properties in the final part, but also during mold filling. Furthermore, the matrix material has a non-Newtonian viscosity behavior, which is also influenced by a phase change, being curing in case of thermoset materials and crystallization or solidifying in case of thermoplastics. The combination of transient matrix viscosity and anisotropy due to fibers leads to complex material behavior, which is hard to handle and to simulate. However, adequate process simulations are needed to ensure and optimize the production and determine the fiber orientation for ongoing structural analysis [1].

For flow modeling, the viscosity is the most important material property. Polymer matrices show temperature- and shear-thinning behavior. Since the focus of this work is on reactive injection molding and hence thermoset materials, the curing kinetics and the accompanying influence on viscosity are also important [2]. For thermoset matrix materials, the mostly used approach for viscosity modeling is the

one presented by Castro and Macosko [3]. As mentioned, besides the matrix, fibers also influence the viscosity of the material during processing. Therefore, the FRP melt is anisotropic with respect to fiber volume fraction Φ_f , length L^f and orientation [4–6]. Similar to solid mechanics, the anisotropy can be represented by a fourth order tensor. However, most state-of-the-art simulation software uses scalar viscosities, and represent the viscosity non-Newtonian and isotropic. Fourth order tensors have for example been used by Sommer et al. [5] for SMC process simulation or in the authors' previous works [7,8] for injection molding simulation. Besides the usage of tensors, there are other approaches to describe the anisotropic character of FRPs during processing. Meyer et al. [9,10] present a meso-scale approach for SMC processing, where the fiber-bundles are represented by solid 1D-element-chains, which interact with the liquid matrix. The fiber orientation and anisotropic stress is thus directly captured by the fluid-structure-interaction of the bundles and the matrix. Furthermore, Favaloro et al. [11] present their IISO-viscosity approach, using fiber orientation tensors and strain rates to calculate a scalar viscosity. Although the viscosity within one element is scalar and therefore isotropic, the anisotropy is considered indirectly due to the dependence

* Corresponding author.

E-mail address: florian.wittemann@kit.edu (F. Wittemann).

<https://doi.org/10.1016/j.jnnfm.2022.104950>

Received 14 July 2022; Received in revised form 3 November 2022; Accepted 8 November 2022

Available online 15 November 2022

0377-0257/© 2022 The Author(s). Published by Elsevier B.V. This is an open access article under the CC BY license (<http://creativecommons.org/licenses/by/4.0/>).

of the scalar viscosity on the different orientation states and strain rates within different elements.

During processing, the fibers orientate depending on the flow field and material behavior. This orientation state is not only important for the final properties of the part, but also for the material behavior during mold filling [7]. In fact, the orientation influences the flow field and vice versa. A first step to determine the fiber (re-)orientation state is the pioneering work of Jeffery [12], describing the motion of ellipsoidal particles in a Newtonian shear flow. Based on this, many different models with different focuses and material aspects for fiber orientation have been published. The most used are the Folgar-Tucker model, introducing an interaction coefficient to enable steady state orientations [13], the reduced strain closure (RSC) model for highly filled materials [14] and the anisotropic rotary diffusion (ARD) model for long fiber materials [15]. Simulating all fibers separately is numerically not sustainable, therefore, most approaches today describe the fiber orientation with orientation tensors, as described by Advani and Tucker [16]. To describe the evolution of an even-order orientation tensor, the orientation tensor of next higher even order is needed, which is determined with a closure approximation [17]. Different approaches with different advantages and disadvantages have been developed in the last decades. Within this work, the so-called IBOF5 closure approximation is used, being a good compromise of accuracy and efficiency [18].

During processing, forces act on fibers, which may lead to fiber breakage. These forces have different sources like for example other fibers (contact forces) and the surrounding fluid (hydrodynamic forces). To model fiber breakage, not only the forces are important but also the mechanisms, which lead to fiber breakage. In literature, the buckling of fibers (due to longitudinal forces) is named as the most important mechanism for fiber breakage [19–21]. Of course, fiber bending (due to transversal forces) is also a mechanism which may lead to fiber breakage, or at least benefits fiber buckling.

One of the first approaches to describe fiber shortening during processing is given by Shon et al. [22], describing the change of fiber length as function of time and an equilibrium fiber length. However, since no process conditions or material properties are considered, this approach is not well suited for injection molding simulation, having a wide range of possible process parameters, materials and mold geometries, influencing the fiber breakage. Two newer approaches by Phelps et al. [21] and Durin et al. [20], consider important aspects like fiber attributes, shear rate and matrix viscosity.

Since the focus of [21] is on injection molding, the present work builds on [21] and combines it with a macroscopic approach for hydrodynamic forces acting on reference fibers in a homogenized material with information provided by the second order orientation tensor [23]. Due to the anisotropic viscosity tensor according to Wittemann et al. [7], the fiber breakage directly influences the viscosity and hence the flow behavior, which is also visible in the predicted cavity pressure. The simulations are carried out with the finite volume based open-source software OpenFOAM.

2. Theory

This section describes the theory and methodology for the novel fiber breakage modeling approach. Section 2.1 describes the modeling of the FRP's viscosity as an fourth order anisotropic tensor, based on our previous work [7]. Section 2.2 described the approximation for the hydrodynamic drag and lift force in case of an homogenized material approach, based on our previous work [23]. Section 2.3.1 shortly describes the fiber breakage modeling approach by Phelps et al. [21]. The novel modeling approach of the present work is the usage of hydrodynamic forces and eigenvectors as reference fibers for fiber breakage modeling, which is described in Section 2.3.2. The main aspect of the present work is the combination of the fiber breakage modeling and the anisotropic flow modeling, so the fiber shortening directly influences the flow modeling.

2.1. Transient non-Newtonian anisotropic viscosity

To model the viscosity of an FRP, the matrix viscosity η_M is described non-Newtonian and with respect to curing kinetics. Therefore, the approach of Castro and Macosko [3] is used within this work, describing η_M with a combination of a Cross type equation for shear dependency and an Arrhenius equation for temperature dependency as well as an additional term for curing dependency so

$$\eta_M = \frac{\eta_0}{1 + \left(\frac{\eta_0 \dot{\gamma}}{\tau^*}\right)^{1-n_{CM}}} \left(\frac{c_g}{c_g - c}\right)^{(c_1+c_2c)} \quad (1)$$

$$\eta_0 = B_{CM} \exp\left(\frac{T_B}{T}\right),$$

where n_{CM} , τ^* , B_{CM} , T_B , c_1 and c_2 are material specific constants. $\dot{\gamma}$ represents the scalar shear rate, being the scalar magnitude of the strain rate tensor \mathbf{D} , T the temperature, c the degree of cure and c_g the gelation conversation point. The curing kinetics are described with the Kamal-Malkin (or Kamal-Sourour) approach [2] within this work. This empirical approach, describes the change rate of cure only as function of time, temperature and actual curing state. There are mechanistic approaches, which describe chemical processes more detailed, but need material-specific information, which requires high experimental effort [24]. The Kamal-Malkin approach is well established and has been successfully used in several scientific publications [7,23,25–27].

For the influence of fibers, one of the first descriptions of anisotropic fluids is given by Gibson [28], presenting the fluidity tensor of a transversely isotropic material. In ongoing studies, Pipes et al. [4] determined the viscosity tensor of a fully aligned FRP as function of fiber volume fraction Φ_f , fiber aspect ratio r_f and matrix viscosity η_M , based on micro-mechanic models. The viscosity is represented by the elongational viscosity η_{11} , axial shear viscosity η_{12} and transverse shear viscosity η_{23} , defined as

$$\eta_{11} = \frac{\eta_M \Phi_f}{2} \left(\frac{\sqrt{\Phi_f/\Phi_{\max}}}{1 - \sqrt{\Phi_f/\Phi_{\max}}} \right) r_f^2$$

$$\eta_{12} = \frac{\eta_M}{2} \left(\frac{2 - \sqrt{\Phi_f/\Phi_{\max}}}{1 - \sqrt{\Phi_f/\Phi_{\max}}} \right), \quad (2)$$

$$\eta_{23} = \frac{\eta_M}{(1 - \Phi_f/\Phi_{\max})^2}$$

with Φ_{\max} being the maximum possible fiber volume fraction, assumed to be $\pi/\sqrt{12}$ (hexagonal packing) [4]. Since hexagonal packing represents a stable equilibrium, it is the more realistic case than square packaging. Within [4] the assumption of incompressibility is made, therefore the parameters mentioned in Eq. (2) fully describe the transversely isotropic fluid. In 2018, Sommer et al. [5] combined the results of Pipes et al. [4] with the orientation averaging approach of Advani and Tucker [16] to fully describe the fourth order viscosity tensor η_{IV} of an FRP with Newtonian matrix by

$$\eta_{IV} = (\eta_{11} - 4\eta_{12} + \eta_{23})\mathbb{A} + \left(-\frac{\eta_{11}}{3} + \eta_{23}\right)(\mathbf{A} \otimes \mathbf{I} + \mathbf{I} \otimes \mathbf{A}) + (\eta_{12} - \eta_{23})(\mathbf{A}\mathbf{I} + (\mathbf{A}\mathbf{I})^{\text{Tr}} + \mathbf{I}\mathbf{A} + (\mathbf{I}\mathbf{A})^{\text{Tr}}) + \left(\frac{\eta_{11}}{9} - \eta_{23}\right)(\mathbf{I} \otimes \mathbf{I}) + \eta_{23}(\mathbf{I}\mathbf{I} + (\mathbf{I}\mathbf{I})^{\text{Tr}}), \quad (3)$$

where \mathbf{A} and \mathbb{A} are the second and fourth order orientation tensor and \mathbf{I} represents the second order unit tensor. The operators are the dyadic product $\otimes ((\mathbf{A} \otimes \mathbf{B})_{ijkl} = A_{ij}B_{kl})$ and the box product $((\mathbf{A}\mathbf{B})_{ijkl} = A_{ik}B_{jl})$.

With this formulation of the viscosity tensor, the viscous stress tensor of the momentum equation τ is given by

$$\tau = \eta_{IV} D. \quad (4)$$

In our previous work [7], Eq. (3) is used for the FRP phase in a multiphase injection molding simulation, considering isotropic air and anisotropic FRP with non-Newtonian matrix behavior. This simulation approach is also used within the present work to model the material's viscosity.

2.2. Calculation of hydrodynamic forces

Several studies in scientific publications offer approaches to model hydrodynamic forces from liquid matrix on fibers. A few examples are Meyer et al. [9], Dinh and Armstrong [29], Phan-Thien et al. [30] as well as Lindström and Uesaka [31]. In the present work, the hydrodynamic forces in the homogenized material are approximated according to the approach presented in our previous work [23], which is briefly described in the following.

2.2.1. Hydrodynamic forces on a fiber

The hydrodynamic force F^{hyd} is split into a drag part F^{d} and a lift part F^{li} . The drag force is a type of fluid friction force, acting on an arbitrary inclusion (a fiber in this case) from a surrounding fluid (matrix) due to relative motion. Unlike most approaches for dry friction, the drag force depends on the relative velocity between inclusion and fluid. The direction is always parallel to the relative velocity. Since fibers are non-spherical bodies, the surrounding fluid also applies a lift force on the inclusion, similar to the aerodynamic force in aeronautics. This force always acts perpendicular to the relative velocity and in a plane defined by the inclusion and relative velocity. Due to the high viscosities and the thin-wall character of the parts, the Reynold's number in injection molding is low in most cases. Therefore, the drag force can be described by Stokes law, determining the drag force on a spherical object in viscous fluid, derived by Stokes in the mid of the nineteenth century. According to Stokes law, the drag force on a spherical body is given by

$$F^{\text{d-sp}} = 3\pi\eta_{\text{M}}d_{\text{sp}}\Delta U, \quad (5)$$

where d_{sp} is the diameter of the spheroid and ΔU is the relative velocity between the inclusion and the surrounding fluid, being fibers and matrix in this case. According to Batchelor [32], the absolute hydrodynamic resistance is proportional to $\eta_{\text{M}}d_{\text{sp}}\|\Delta U\|$ and independent of the body's shape, therefore Meyer et al. [9] present an approximation for cylindrical bodies (fibers) with a dimensionless correction coefficient k_{d} , being defined as function of fiber aspect ratio and relative angle between fiber and relative velocity ϕ , so

$$k_{\text{d}} = 1 - \alpha(r_{\text{f}} - 1)\cos(2\phi) + \beta(r_{\text{f}} - 1), \quad (6)$$

with $\alpha = 0.09$ and $\beta = 0.3125$. Finally, the drag force for fibers is defined as

$$F^{\text{d}} = 3\pi\eta_{\text{M}}k_{\text{d}}(r_{\text{f}}, \phi)d_{\text{f}}\Delta U. \quad (7)$$

Similar to the drag force, Meyer et al. [9] approximate the lift force by

$$F^{\text{li}} = 3\pi\eta_{\text{M}}k_{\text{li}}(r_{\text{f}}, \phi)d_{\text{f}}\|\Delta U\|[\mathbf{q}], \quad (8)$$

with

$$k_{\text{li}} = \alpha(r_{\text{f}} - 1)\sin(2\phi). \quad (9)$$

The vector \mathbf{q} defines the direction of the lift force and the brackets $[\cdot]$ indicate that the vector is normed. The definitions of k_{d} and k_{li} represent a best fit for numerical experiments. Within [9], mesoscopic simulations of simple shear flows with different fiber orientations and different

aspect ratios are performed to compute the stress on the fiber surface. The resulting forces are set in relation to Eq. (7) and Eq. (8) to determine k_{d} and k_{li} .

Finally, the complete hydrodynamic force acting from the liquid matrix on a fiber is given by

$$F^{\text{hyd}} = F^{\text{d}} + F^{\text{li}} = 3\pi\eta_{\text{M}}d_{\text{f}}(k_{\text{d}}(r_{\text{f}}, \phi)\Delta U + k_{\text{li}}(r_{\text{f}}, \phi)\|\Delta U\|[\mathbf{q}]). \quad (10)$$

2.2.2. Hydrodynamic forces for homogenized material

According to Eq. (10), the information needed to calculate F^{hyd} are, among others, the relative velocity between the fibers and the fluid, and the according angle between the fiber and the relative velocity, which are both not directly available in a homogenized material approach with orientation tensors, since no exact fiber orientation is given. In our previous work [23], we present an approach to determine the average hydrodynamic forces with information provided by the second order orientation tensor. The eigenvectors ν are regarded as reference fibers, so there are always three reference fibers ν_k separated by the index $k \in \{1, 2, 3\}$ in each cell, with an explicit, individual and known orientation direction.

Based on the eigenvectors, the angle between the relative velocity and the fiber is given by

$$\phi_k = \arccos\left(\frac{\Delta U \cdot \nu_k}{\|\Delta U\|}\right). \quad (11)$$

The vector \mathbf{q} , representing the direction of the lift force is given by

$$\mathbf{q}_k = (\nu_k \times [\Delta U]) \times [\Delta U]. \quad (12)$$

Both quantities are calculated three times in each cell, once for each eigenvector ν_k .

To approximate the relative velocity, it is assumed, that all fibers within one cell have on average the velocity of the cell center. This assumption is supported by the fact, that otherwise fiber matrix separation would occur, which is neglected within the simulation [23]. The relative velocity can be approximated by

$$\Delta U = \sum_l^{l_{\text{max}}} \frac{w_{l0}}{W_o} (U_l - U_o), \quad (13)$$

with $w_{l0} = \exp(-9d_{l0}^2/(2(L^f)^2))$ and $W_o = \sum_l^{l_{\text{max}}} w_{l0}$. Here, the index o represents the regarded origin cell, l represents the l -th of the l_{max} regarded neighbor cells and L^f is the fiber length. d_{l0} is the distance between the cell centers of cells o and l . Hence, ΔU is calculated with the velocities U_l of the l_{max} considered neighbor cells. The number of regarded neighbors is chosen so the average distance is $1/l_{\text{max}} \sum_l^{l_{\text{max}}} d_{l0} \geq 1.5 L_n^i$. The index n indicates different fiber lengths. This formulation is identical to [9,23] since the hydrodynamic force is a kind of long range interaction and a satisfactory number of surrounding cells should be taken into account, especially when the considered fiber length extend cell sizes. Therefore, the velocity gradient would not be representative, but it can be used to model short range interactions, acting on a smaller scale like fiber-fiber friction and lubrication force, as shown in our previous work [23].

This approach to approximate the hydrodynamic force was verified with numerical experiments in [23]. The hydrodynamic force was determined for 22 different orientation states and relative velocities of 500 randomly created fibers and the corresponding orientation tensor. The average force of every orientation state is given correctly by regarding only the eigenvectors of the orientation tensor as reference fibers. However, there is no possibility on macroscopic scale to infer the individual forces acting on single fibers, when using the orientation tensor.

2.3. Fiber breakage modeling

The hydrodynamic forces are used for fiber breakage modeling.

Although approaches exist to approximate the fiber-fiber friction and lubrication force [23], the exact mechanisms of these forces in highly filled materials are not well understood at this point of time. Therefore, they are neglected within this work. The assumptions for the fiber breakage model are in accordance with the model of Phelps et al. [21]:

- Fibers break only due to buckling
- Fibers break only in one point, so one fiber breaks only in two parts
- Until buckling, fibers are perfect, rigid cylinders
- There is a defined minimum fiber length, which cannot be undercut
- There is a defined number of possible fiber lengths.

The following Section 2.3.1 briefly describes the fiber breakage modeling approach of Phelps et al. [21]. The ongoing Section 2.3.2 describes the novel fiber breakage modeling approach of the present work, which is based on [21], but with force calculation based the hydrodynamic force approximation explained Section 2.2 and the usage of eigenvectors and eigenvalues to determine the breakage probability to create a more orientation dependent calculation.

2.3.1. Fiber breakage modeling in injection molding simulations with homogenized material approach

Phelps et al. [21] assume that fibers break in only two parts. They further consider buckling as the only mechanism for fiber breakage and buckling due to the Euler buckling theory, so critical force for buckling F_{bu} by

$$F_{bu} = \frac{\pi^3 E_f d_f^4}{64 (L^f)^4}, \quad (14)$$

with E_f , L^f and d_f being the elastic modulus, length and diameter of the fiber. Based on the slender body analysis of Dinh and Armstrong [29], a force F_f acting on the fibers is given by

$$F_f = \frac{\zeta \eta_M \dot{\gamma} (L^f)^2}{8} (-D : (\mathbf{p} \otimes \mathbf{p})), \quad (15)$$

where ζ is a dimensionless and empirical drag coefficient and \mathbf{p} is a single fiber orientation direction. For fiber breakage, a so called buckling index B_n^{bu} is defined as

$$B_n^{bu} = \frac{F_f}{F_{bu}} = \frac{4\zeta \eta_M \dot{\gamma} (L_n^f)^4}{\pi^3 E_f d_f^4}, \quad (16)$$

by assuming $(-2D : (\mathbf{p} \otimes \mathbf{p}))/\dot{\gamma} = 1$. The index n indicates different fiber lengths L_n^f , which may occur. To model the fiber shortening, Phelps et al. define a breakage probability

$$P_n^{br} = \begin{cases} 0 & \text{for } B_n^{bu} < 1 \\ C_{br} \dot{\gamma} (1 - \exp(1 - B_n^{bu})) & \text{for } B_n^{bu} \geq 1 \end{cases} \quad (17)$$

for every fiber length, where C_{br} is an empirical breakage coefficient.

The breakage of fibers creates new, shorter fibers. Therefore, Phelps et al. [21] define a child generation rate R_{nm}^{br} with a Gaussian probability function (PDF), which also describes the breakage point along the fiber so

$$R_{nm}^{br} = \varrho_m^{br} \text{PDF}\left(L_n^f, \frac{L_m^f}{2}, S_{br}\right), \quad (18)$$

with standard deviation S_{br} and mean value $L_m^f/2$. The scaling factor ϱ_m^{br} is defined to fulfill a continuity condition, defined in [21]. It is $R_{nm}^{br} = R_{(m-n)m}^{br}$ since the lengths of one child n and the parent fiber m define the length of the other child fiber. For example, it is $R_{25}^{br} = R_{35}^{br}$ representing the probability, that a fiber of length L_5^f breaks into two children with the lengths L_2^f and L_3^f . Furthermore, it is $R_{nm}^{br} = 0$ for $L_n^f \geq L_m^f$, so short

fibers cannot recombine to longer fibers again.

Finally, Phelps et al. describe the evolution of fiber lengths by

$$\frac{\partial N_n^f}{\partial t} + U_i \frac{\partial N_n^f}{\partial x_i} = -P_n^{br} N_n^f + \sum_m P_{nm}^{br} N_m^f, \quad (19)$$

where N_n^f represents the number of fibers with length L_n^f and U_i is the velocity vector.

2.3.2. Novel breakage modeling approach based on hydrodynamic forces

In a first step, it is determined, if the reference fiber is under compression, so buckling is possible, or under tension. For the latter case no fiber damage is considered. The identification of the fiber being under compression (Fig. 1 blue region) or tension (Fig. 1 red region) is depending on the orientation of the fiber and the flow field, presented by Jeffery in 1922 [12]. Fig. 1 visualizes whether the fibers is under compression or tension on a unity sphere for a normed shear flow. The fiber (or eigenvector in this case) is under compression and able to buckle if

$$D : (\boldsymbol{\nu} \otimes \boldsymbol{\nu}) < 0. \quad (20)$$

In a second step, the force acting on the reference fiber is determined. For Euler buckling theory, only the force component in fiber direction is relevant and the forces only act at the fiber ends, so the force is given by

$$\hat{F}_{kn}^{hyd} = \boldsymbol{\nu}_k : \mathbf{F}_n^{hyd}. \quad (21)$$

The buckling criterion is reached if

$$B_{kn}^{hyd} = \frac{\hat{F}_{kn}^{hyd}}{F_n^{bu}} \geq 1, \quad (22)$$

with F_n^{bu} being the critical force for a fiber with length L_n^f and defined in Eq.(14).

Afterwards, a breakage probability P_{kn}^{br} is determined for every eigenvector $\boldsymbol{\nu}_{ik}$ and fiber length L_n^f by

$$P_{kn}^{hyd} = \begin{cases} 0, & B_{kn}^{hyd} < 1 \quad \text{or} \quad D : (\boldsymbol{\nu} \otimes \boldsymbol{\nu}) \geq 0 \\ C_{br} \dot{\gamma} (1 - \exp(1 - B_{kn}^{hyd})), & B_{kn}^{hyd} \geq 1 \quad \text{and} \quad D : (\boldsymbol{\nu} \otimes \boldsymbol{\nu}) < 0 \end{cases} \quad (23)$$

The definition P_{kn} is similar to the one given by Phelps et al. [21] (Eq. (17)), but calculated three times within one cell in this work, once for every eigenvector and depending on the orientation of the eigenvector. To sum up the breakage probability for one fiber length within one cell, the individual P_{kn} are weighted with the eigenvalues of the orientation tensor, representing the amount of fibers with the corresponding orientation state, so

$$P_n^{hyd} = \lambda_k P_{kn}^{hyd}, \quad (24)$$

where λ_k are the eigenvalues.

The ongoing fiber breakage modeling is similar to the method of Phelps et al. [21]. The child generation is given by Eq. (18) and the evolution is given by Eq.(19).

3. Results, experimental validation and discussion

3.1. Orientation dependency of the novel approach

To highlight the orientation dependency of the novel approach, a simple shear flow is simulated and the approach is compared to the state-of-the-art approach presented in [21]. However, the two approaches are not directly comparable, since the force calculation is different and the state-of-the-art approach needs an empirical parameter to determine the force acting on the fibers. Therefore, the focus of comparison will be orientation dependency and the results are normed,

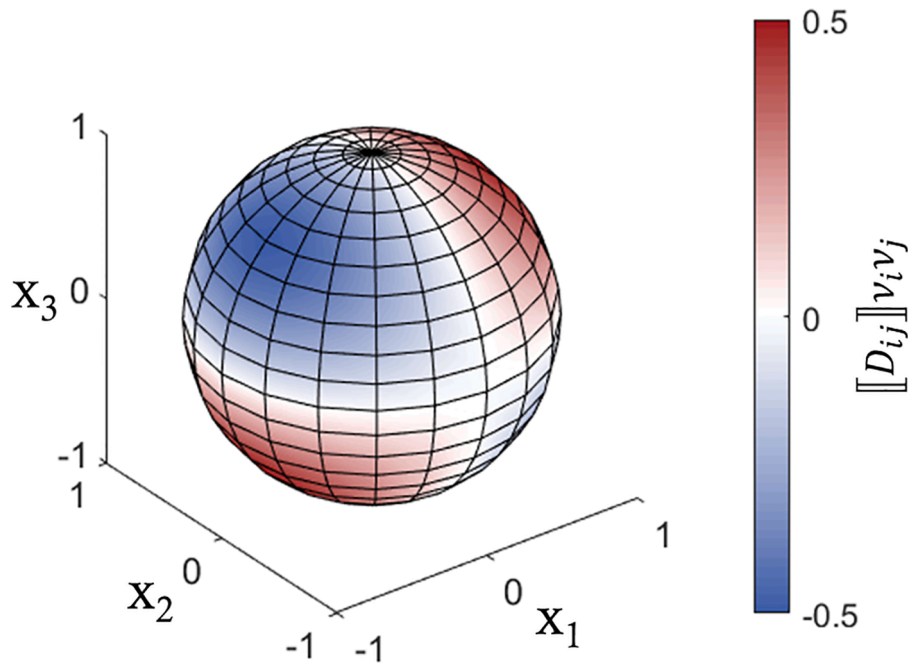


Fig. 1. Unity sphere in simple shear flow, whether the fibers is under compression (blue regions) or tension (red regions) by values of $D : (\nu \otimes \nu)$.

which is an idealized and theoretical case.

The parameters needed for the simple shear flow simulation are given in Table 1, to keep the case as simple as possible, the viscosity is represented isotropic and Newtonian by the value η_c . The values are chosen to correspond to a real injection molding process, the fiber orientation is modeled with the RSC-model [14], and the parameters are identical to the values used in the experimental validation.

According to the parameters given in Table 1 the fibers will orientate slightly in flow direction (x_3 -direction) over time, where most of the fibers are under tension and not able to buckle [21]. Fig. 2, shows the amount of fibers, being able to buckle in the corresponding orientation state and flow field. This amount is calculated by summing up the eigenvalues of A , if the corresponding eigenvector fulfills the condition in Eq. (20). This amount decreases over time due to higher amount of fibers with orientation steady-state orientation.

Additionally, Fig. 2 shows the normed breakage probability of the novel, orientation dependent approach, based on hydrodynamic forces as well as the normed breakage probability of the state-of-the-art approach. The values are normed since their absolute value is not directly comparable due to the different force calculation and the focus is to highlight the orientation dependency of the novel approach.

Due to the constant strain rate tensor and corresponding constant scalar shear rate $\dot{\gamma}_0 = 100$ 1/s, the breakage probability in the state-of-the-art approach (Eq. (16) and Eq. (17)) is constant over time and the change of orientation is not captured. In the hydrodynamic based approach, the force calculation (Eq. (10)) and breakage probability (Eq. (24)) depend on orientation and therefore the breakage probability decreases over time due to the smaller amount of buckling fibers and computed acting force. The change of the breakage probability is more

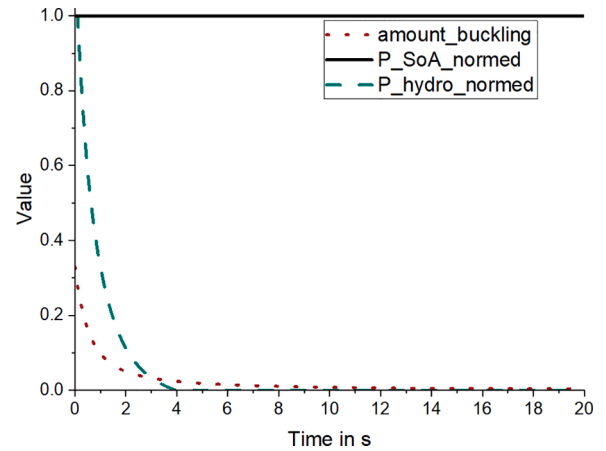


Fig. 2. Amount of fibers able to buckle (rad, dotted), normed breakage probability with state-of-the-art model (black, solid) and normed breakage probability with novel approach (green, dashed) over time in simple shear flow with parameters given in Table 1.

sensitive towards the change of orientation compared to the amount of buckling fibers, due to the non-linear dependence of force calculation to orientation. Fig. 2 highlights the orientation dependency of the novel approach which is the main benefit compared to the state-of-the-art.

3.2. Experimental setup and simulation model

The fiber breakage and flow modeling are validated with injection molding experiments of a 480 mm x 190 mm x 4 mm rectangle plate. The material enters the plate via a cone sprue in the center, having a start diameter of 9 mm, an end diameter of 15.5 mm and a length of 185 mm. For validation, two sensors measure the cavity pressure during mold filling and specimens are taken for fiber length measurement. The cavity with a part of the screw chamber and the positions of the sensors is shown in Fig. 3.

The experiments are performed by Maertens et al. [33]. The used injection molding machine is a KraussMaffei 550/2000 GX with a

Table 1

Parameters for simulating the simple shear flow.

Parameter	Value	Unit
η_c	500	Pa•s
D_{23}, D_{32}	100	1/s
$D_{11}, D_{12}, D_{13}, D_{21}, D_{22}, D_{31}, D_{33}$	0	1/s
Initial orientation state		
A_{11}, A_{22}, A_{33}	1/3	-
$A_{12}, A_{13}, A_{21}, A_{23}, A_{31}, A_{32}$	0	-

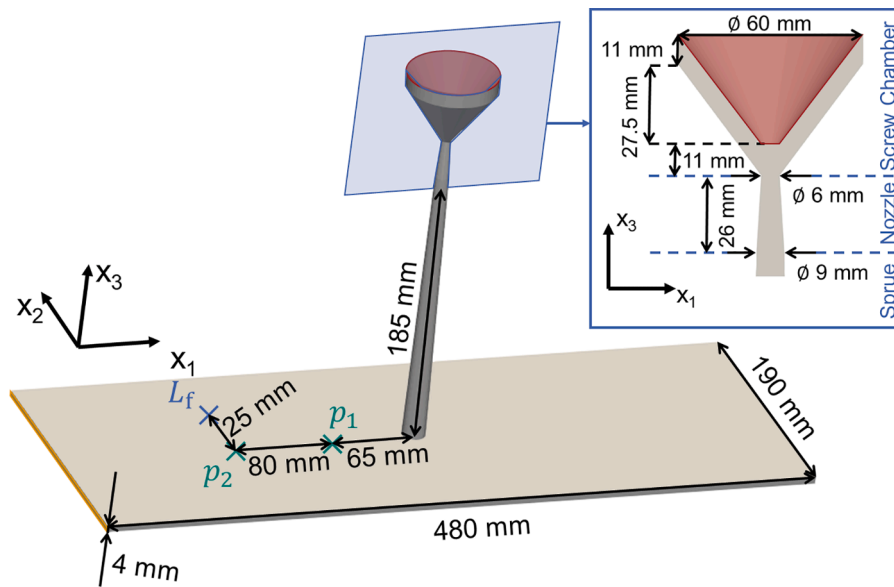


Fig. 3. Cavity with positions of pressure sensors p_1 and p_2 , position for fiber length evaluation L_f for validation. Inlet area in red and outlet in orange.

standard 60 mm screw. The used material is a phenolic molding compound of novolac type, filled with 55%-weight glass fibers, named Porophen GF9201L12a by Sumitomo Bakelite Co., Ltd. The initial fiber length in material is $L_{f0} = 12$ mm.

For fiber length measurement, specimens are extracted from the plate (Fig. 3 position L_f) and from the frontal part of the screw chamber. The latter ones are extracted to get the fiber length distribution after plastification, directly before the material enters the cavity, since significant proportion of fiber shortening happens during plastification, when the material is transported by the screw. As described in [33], after the specimens are extracted, the matrix is removed by pyrolysis and the residue is transferred into an aqueous solution for dilution. Samples of the dilution are measured by optical fiber detection of the commercially available FASEP system by IDM Systems, Darmstadt, Germany.

For the simulation, the complete cavity with a small part of the screw chamber is modeled, as illustrated in Fig. 3. The whole model is meshed with hexahedral elements. For the plate, the cell size is of 2.3 mm in x_1 -, 1.75 mm in x_2 - and 0.4 mm in x_3 -direction. The nozzle and sprue are discretized with 32 cells along the circumference, 24 along the diameter and 140 in x_3 -direction. For the screw chamber, 64 cells along the circumference and 72 cells in radial direction are used, with a x_3 -dimension of the cells of 1.57 mm.

The foremost section of the screw chamber is part of the simulation model to create a more realistic material state at the beginning of the sprue with respect to fiber orientation, temperature distribution and of course, fiber length distribution. Therefore, the specimens taken from the screw chamber are used to determine the initial fiber length distribution in the simulation. The matrix viscosity is modeled with Eq. (1), the corresponding parameters are given in Table 2.

The compound viscosity is given by the fourth order viscosity tensor (Eq. (3)) and the fiber orientation is calculated with the RSC model. A

Table 2
Used parameters of the Castro-Macosko model for matrix viscosity.

Parameter	Value	Unit
τ^*	0.0018	Pa
n_{CM}	0.54	-
c_1	5	-
c_2	5	-
B_{CM}	$1.123 \cdot 10^{-7}$	Pa·s
T_B	13,750	K
c_g	0.4	-

detailed description and validation of the anisotropic viscosity model is presented in the previous work [7]. To calculate the viscosity tensor in a simulation with fiber length distribution, the average fiber length in the cell is used.

The parameters for fiber breakage modeling according to Eq. (18) and Eq. (23) are given in Table 3. The material is injected with a constant volume flow of $150 \text{ cm}^3/\text{s}$ and has a melt temperature of $120 \text{ }^\circ\text{C}$. The temperature at the walls is constant $175 \text{ }^\circ\text{C}$.

3.3. Results

3.3.1. Fiber length distribution

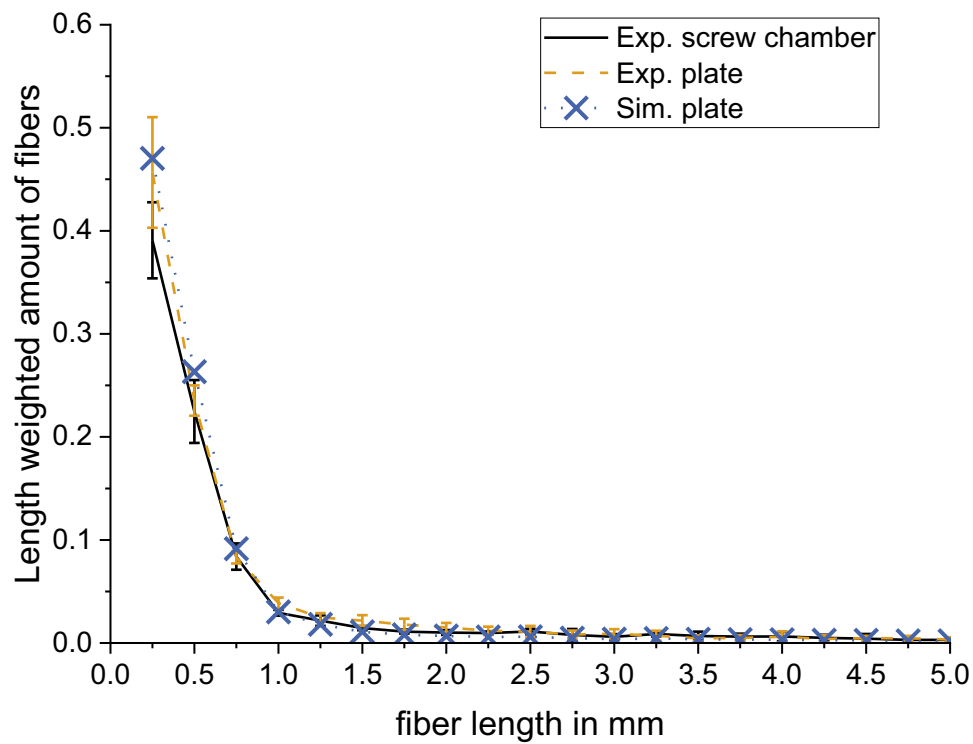
The results of the fiber length distribution are shown in Fig. 4. The possible fiber lengths L_n^f in the simulation are chosen in 0.25 mm steps. Hence the possible lengths in the simulation are between 0.25 mm (shortest) and 12 mm (longest), resulting in 48 possible fiber lengths. The experimental data is clustered so the mean values of the cluster fits to the possible fiber lengths of the simulation. The results are shown with standard deviation in Fig. 4.

The illustration of the results is separated in two graphs, one with fiber lengths from 0.25 mm to 5 mm (Fig. 4a) and one with lengths from 5 mm to 12 mm (Fig. 4b), with different scales on the ordinate axis. The ordinate axis represents the amount of the corresponding fiber length, weighted by length. The results are shown weighted by length only due to visualization. All other average values and calculated average lengths presented by the number average, which is also used in the simulation. Only a small amount of about 4% of the fibers with 11.75 mm or 12 mm remains after plastification. There are some higher values with lengths about 6.25 mm to 8.25 mm. In summary, about 13.6% of the fibers remain with a length > 5 mm, but the majority of the fibers (about 72%) has already broken down to lengths of 1 mm or less before entering the mold (Fig. 4, black curve).

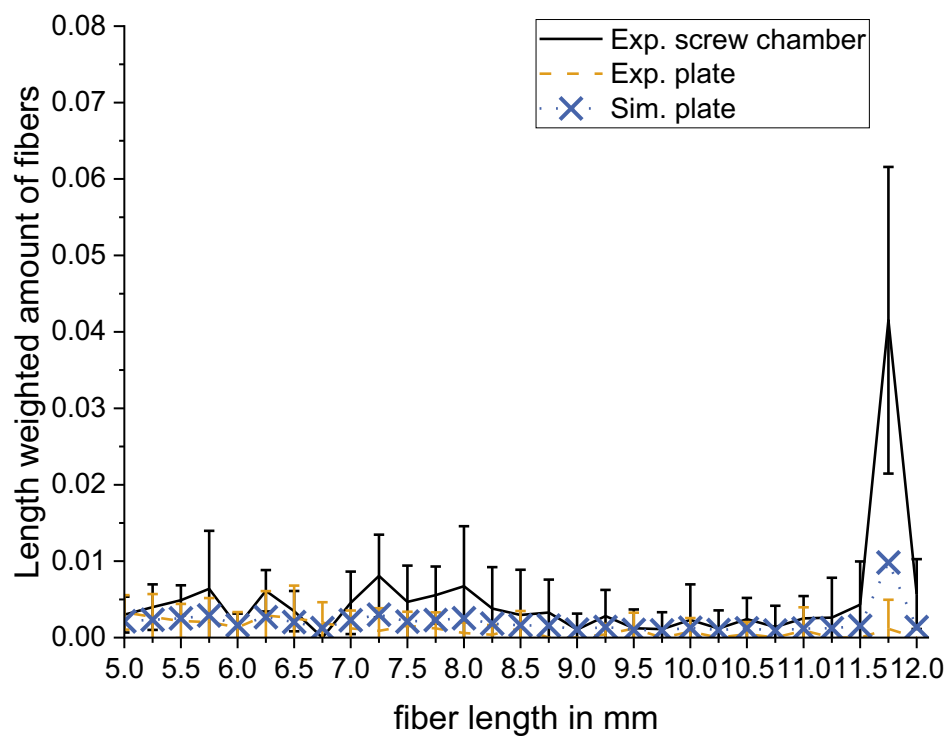
However, there is further fiber breakage during mold filling, shown

Table 3
Used parameters for fiber breakage modeling.

Parameter	Value	Unit
E_f	73	GPa
d_f	$17 \cdot 10^{-6}$	m
C_{br}	0.05	-
S	1	-



(a)



(b)

Fig. 4. Fiber length distribution, weighted by length. Comparison of experimental results (screw chamber in black, plate in orange) and simulation (plate in blue) for fiber lengths from 0.25 to 5 mm (a) and 5 to 12 mm (b).

by the experimental results, extracted from the plate (Fig. 4, orange). Only about 3% of the fibers at the measure area have a length of > 5 mm, and about 81.3% have broken to lengths of 1 mm or less.

The simulation results (Fig. 4, blue) fit well to the experimental results, but slightly overestimate the fiber breakage at low fiber lengths

and underestimate the fiber breakage at fiber lengths > 5 mm. About 85.5% of the fibers have a length of 1 mm or less at the end of the simulation and about 5.6% with a length > 5 mm remain. Especially the amount of fibers remaining at 11.75 mm is overestimated in the simulation, while the amount of fibers with intermediate lengths between 1

mm and 5 mm is underestimated. Weighted by number and with respect to the measurement area, the average fiber length reduces from 0.452 mm to 0.398 mm in the experiments, while it reduces from 0.452 mm to 0.383 mm in the simulation, being a difference of about 4%. For most fiber lengths, the simulation results are within the process and measure uncertainties, shown by the standard deviation in Fig. 4.

Fig. 5 shows the average fiber length and corresponding magnitude of ΔU in the simulation at the x_2 -plane of symmetry. A detailed view on the nozzle and the transition from sprue to the plate is given, being critical positions for fiber breakage due to the high changes in velocity, as highlighted by the magnitude of ΔU .

The average length reduces from the initial value of 0.452 mm to about 0.42 mm in the area directly after the screw chamber. Therefore, the fiber length is already reduced by about 7.6% before reaching the sprue. At the transition from the sprue to the plate, the average fiber length reduces from about 0.42 mm to 0.404 mm, being again about 4%. After the transition into the plate, the average fiber length stays nearly the same, hence, not many fibers break within the plate, due to the simple geometry and flow field. The magnitude of ΔU fits to these results, being high in regions where fibers break and the average fiber length is reduced and low in regions where less fibers break.

3.3.2. In-mold pressure

The experimental pressure at two points in the mold is shown in Fig. 6. The measurement points are highlighted in Fig. 3. Two simulations are performed, one with fiber breakage modeling (Fig. 6, green) and one without (Fig. 6, red). For the simulation without fiber breakage a constant fiber length of 0.452 mm is assumed, being the average fiber length of the measurements taken from the screw chamber. The simulation with fiber breakage predicts the pressure at position p_1 well and slightly too high at position p_2 , but within the process and measuring scatter.

The simulation without fiber breakage predicts a too high pressure at both positions, due to the longer fibers, rising the modelled viscosity. Besides the fiber length, both simulations are completely identical. The parameters given in Table 2 have been identified to fit for the simulation with fiber breakage. Of course, there exists also a parameter set for which the simulation without fiber breakage fits better to the experimental data, but the simulation is performed to be set in relation to the simulation with breakage, not to fit to the experimental results. At the end of filling, the simulation with fiber breakage predicts a pressure of 3.74 MPa at position p_1 and 1.96 MPa at position p_2 . The simulation without breakage predicts 5.04 MPa at position p_1 and 2.63 MPa at

position p_2 , being a difference of about 25.8% and 25.5% at these positions.

Fig. 7 shows the simulated pressure distribution in the nozzle and sprue for both simulations, just before the end of filling. As mentioned in Section 3.3.1, most of the fiber breakage takes place within this part of the mold. For the simulation with fiber breakage, the pressure changes from about 30 MPa at the inlet to about 3.85 MPa at the end of the sprue, being a change of 26.15 MPa (87.17%). For the simulation without fiber breakage, the pressure changes from 36.7 MPa to 5 MPa, being a change of about 31.7 MPa (86.4%). Similar to the positions of the sensors the pressure in the simulation is continuously higher, due to the higher viscosity. At the inlet the pressure is 6.7 MPa (18.2%) higher for the simulation with constant fiber length, at the end of the sprue it is 1.15 MPa (23%) higher.

3.4. Discussion

3.4.1. Fiber length distribution and breakage modeling

The fiber breakage modeling, based on eigenvectors and hydrodynamic forces predicts the fiber length distribution in the part well, having a deviation of about 4% for the average fiber length compared to the experimental results. One negative aspect of the model is the high amount of fibers remaining with a length of 11.75 mm. One reason might be the homogenization. In the real process, for fibers with dimension greater than the part dimension (plate thickness: 4 mm) phenomena like interaction with the wall become very important and may lead to fiber damaging. Furthermore, an out-of-plane orientation for such long fibers is impossible in the real mold. Both aspects are not captured in the simulation at this moment. Only one orientation tensor is determined within a cell and the average fiber length is used to calculate it. Thus, out-of-plane orientation is possible in the simulation, although the values are small. The consideration of wall interactions affects the breaking behavior for every fiber length and is an important aspect for future works.

Fig. 5 identifies the transition between screw chamber and nozzle as well as between sprue and plate as critical areas for fiber breakage. This highlights the importance of considering the screw chamber in the simulation model. In a state of the art simulation, the model would begin at the beginning of the sprue, where an amount of fibers have already been broken. In the simulation, the average fiber length reduces by about 7.6% in this area, so even if the length distribution after plastification is known, this distribution is no longer accurate at the beginning of the sprue.

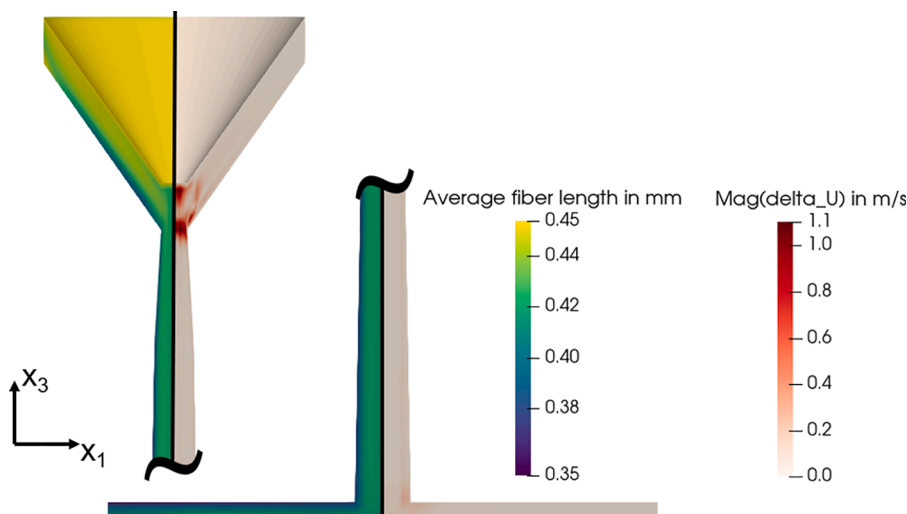


Fig. 5. Average fiber length and magnitude of ΔU at the x_2 -plane of symmetry in the simulation model. Detailed illustration of the nozzle and the transition from sprue to plate.

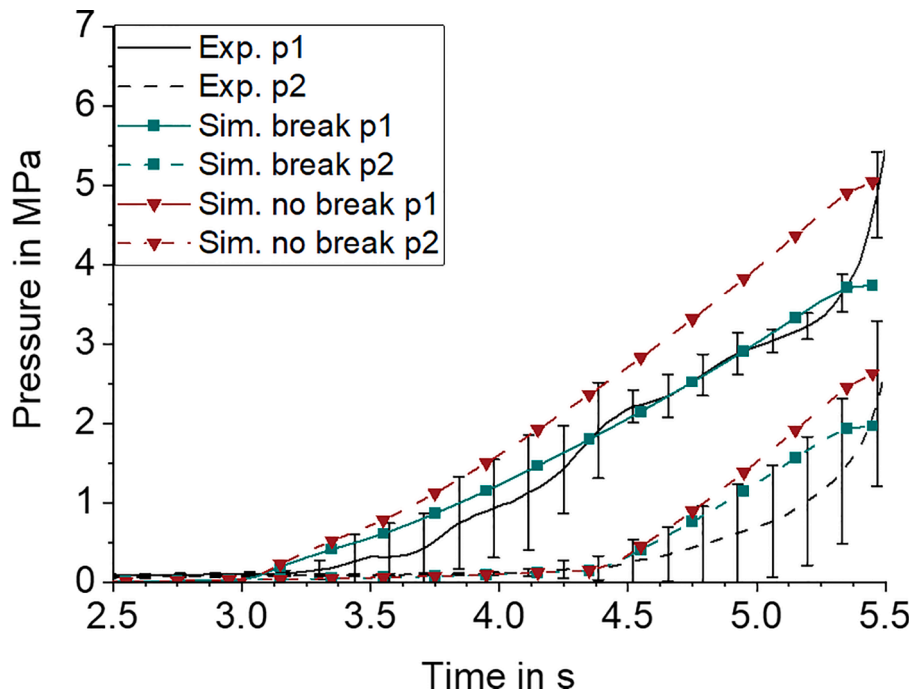


Fig. 6. In-mold pressure during filling over time for experiment (black), simulation with fiber breakage (green, squares) and without fiber breakage (red, triangles). Solid lines represent position p_1 , dashed lines position p_2 (cf. Fig. 3).

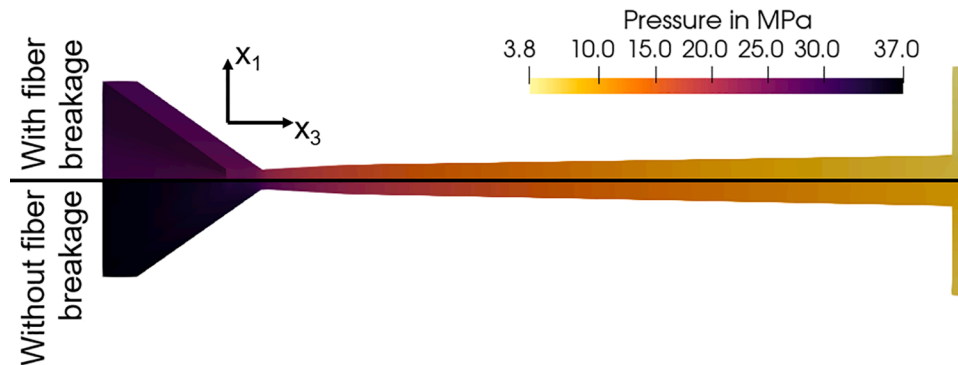


Fig. 7. Simulated pressure distribution in the nozzle and sprue for simulation with fiber breakage (top) and without fiber breakage (bottom).

3.4.2. In-mold pressure modeling

The simulation with fiber breakage predicts the pressure well at both positions. Although the pressure is slightly too high at position p_2 , it is within the process and measuring scatter over the whole time. This validates the approach to simulate the mold filling process with transient fiber length and orientation-dependent viscosity modeling. The comparison of the simulations with and without fiber breakage modeling highlights the influence of the fiber length on the flow behavior. In the simulation with constant fiber length, the pressure is higher at every point, since the longer fibers rise the viscosity, by rising the parameter η_{11} as given by Eq. (2). In the simulation with fiber breakage, the shortening of fibers lowers the viscosity, and therefore the absolute pressure as well as the pressure drop decrease. At the end of filling, the two simulations deviate by about 25.8% and 25.5% at the sensor positions. The deviation is quite similar, since not much fiber breakage occurs in the area between the two pressure sensors. As shown in Fig. 5 and explained in Section 3.3.1 the majority of fiber breakage is happening before the material enters the plate, where also a difference in pressure between the simulations is detectable (cf. Fig. 7). As given in Eq. (2), the fiber lengths influence the calculation of η_{11} by second order and therefore the viscosity and hence the predicted pressure are

sensitive towards the fiber length. Older studies like the one from Brodnyan [34] and Ziegel and Eirich [35] also report a non-linear relation between effective viscosity and the aspect ratio of inclusions. Kitano et al. [36] also report a second order correlation between the effective viscosity of an FRP and the aspect ratio of the fibers. At the end of filling, the average fiber length in the whole model is 0.396 mm, while it is still 0.452 mm in the simulation without fiber breakage. The squares of these two values deviate by 23.3%. At the end of the sprue, the squares of the fiber lengths differ by about 20.1%, while the pressure difference is 23%. At the sensor positions the squares of fiber lengths differ by about 28.2% and the pressure by 25.5%. Of course, the deviation of fiber length cannot be set in direct correlation to the modeled pressure, but it is in a meaningful magnitude.

The difference between both simulations highlights the benefit and importance of fiber breakage modeling for accurate injection molding process simulations. The material behavior is sensitive towards fiber length, not only for the structural behavior of the final part, but also during processing. Besides the more adequate flow and mold filling modeling, the process-induced fiber length distribution is an important input for ongoing analysis of warpage and structural behavior.

4. Conclusion and outlook

A novel simulation approach for fiber-dependent flow modeling in injection molding simulation is presented. The approach uses a fourth-order viscosity tensor, considering matrix viscosity as well as fiber volume fraction, fiber orientation and length to model the viscosity of the FRP. This approach is combined with a novel approach for fiber breakage modeling, based on the calculation of hydrodynamic forces, acting from the fluid on the fibers. The approach is based on the work of Phelps et al. [21] with two main differences. One is a different force calculation, reducing the need of model parameters by one. The other difference is the relation of force and breakage probability to the eigenvectors and eigenvalues, enabling orientation-dependent calculation of these two values and the possibility, that only a part of the fibers within one cell buckles and breaks. Due to the consideration of the fiber length in the flow modeling, the fiber breakage directly influences the viscosity and hence flow modeling. The complete simulation can be performed with information provided by the second order orientation tensor.

The approach is validated with experimental data of reactive injection molding trials with a long glass fiber filled phenolic compound. The predicted fiber length distribution and in-mold pressure of the simulation model fit well to the experimental results. Furthermore, the simulation is compared to a simulation with constant fiber length, highlighting the influence of fiber breaking on the flow modeling and the importance of fiber breakage modeling for accurate injection molding process simulations. The deviation of the predicted pressure of the two simulations is in a meaningful magnitude compared to the shortening of fibers. Besides the more adequate flow and mold filling modeling, the process-induced fiber length distribution is an important input for warpage and structural simulations.

Although the results fit well to experimental data, the modeling approach and results can still be improved by considering further phenomena. One aspect is the consideration of wall interaction, which has a high impact especially for behavior of longer fibers. This may improve the simulation results, since breakage of longer fibers in the simulation is too low compared to the experimental results. Another aspect are further investigations in interaction and contact forces between fibers, which are especially relevant in concentrated suspensions, where fibers could have multiple contact points to other fibers. Friction, lubrication and normal force appear at these contact points and influence the rheological behavior of the material as well as the fiber orientation and breakage evolution. However, the influence of these forces on the material behavior is not well understood at this point of time. More investigation needs to be done on the experimental and numerical side. Microscopic simulation, considering single fibers may give more information about the impact of fiber-fiber forces and contacts on the macroscopic behavior of the material. Within this work, the number average is used to determine the average fiber length, which is used to determine the viscosity tensor. Studies of Pipes et al. [37] and Shuler et al. [38] show that the rheological behavior of an FRP with multiple fiber lengths can be adequately represented by the average, but already small amounts of long fibers in a suspension have high impact on the materials rheological behavior. Therefore, further investigations on the usage of the fiber length distribution for viscosity modeling within the presented approach are also an interesting aspect.

Author contributions

Florian Wittemann performed the major part of the work in terms of method development and implementation. He also wrote the first draft of the paper. Luise Kärger supervised the method development, supported the discussion of simulation results and thoroughly revised the paper. Frank Henning supervised the work in terms of composite process knowledge and scientific relevance of the addressed subjects.

Declaration of Competing Interest

The authors declare the following financial interests/personal relationships which may be considered as potential competing interests: Luise Kaerger reports financial support was provided by German Research Foundation. Frank Henning reports financial support was provided by State of Baden-Württemberg Ministry for Science Research and Art.

Data availability

Data will be made available on request.

Acknowledgments

We would like to thank the 'Deutsche Forschungsgemeinschaft' (DFG) for funding the research project 'MeproSi' (project number: 464119659), which enabled this work. Furthermore, the here proposed methods have been applied within the framework of the funded project ReMoS within the Innovationscampus Mobilität der Zukunft. ReMoS is funded by the Ministry of Science, Research and Art of the state Baden-Württemberg, which we also thank for the funding and financial support.

References

- [1] J. Görthofer, N. Meyer, T.D. Pallicity, L. Schöttl, A. Trauth, M. Schemmann, M. Hohberg, P. Pinter, P. Elsner, F. Henning, A. Hrymak, T. Seelig, K. Weidenmann, L. Kärger, T. Böhlke, Virtual process chain of sheet molding compound: development, validation and perspectives, *Compos. B Eng.* 169 (2019) 133–147, <https://doi.org/10.1016/j.compositesb.2019.04.001>.
- [2] M.R. Kamal, S. Sourour, Kinetics and thermal characterization of thermoset cure, *Polym Eng Sci* 13 (1973) 59–64, <https://doi.org/10.1002/pen.760130110>.
- [3] J.M. Castro, C.W. Macosko, Studies of mold filling and curing in the reaction injection molding process, *Am. Instit. Chem. Eng. J.* 28 (1982) 250–260, <https://doi.org/10.1002/aic.690280213>.
- [4] R.B. Pipes, J.W.S. Hearle, A.J. Beaussart, A.M. Sastry, R.K. Okine, A Constitutive Relation for the Viscous Flow of an Oriented Fiber Assembly, *J. Compos. Mater.* 25 (1991) 1204–1217, <https://doi.org/10.1177/002199839102500907>.
- [5] D.E. Sommer, A.J. Favaloro, R.B. Pipes, Coupling anisotropic viscosity and fiber orientation in applications to squeeze flow, *J. Rheol. (N Y N Y)* 62 (2018) 669–679, <https://doi.org/10.1122/1.5013098>.
- [6] S.G. Advani, *Flow and Rheology in Polymer Composites Manufacturing*, Elsevier, Amsterdam, New York, 1994.
- [7] F. Wittemann, R. Maertens, L. Kärger, F. Henning, Injection molding simulation of short fiber reinforced thermosets with anisotropic and non-Newtonian flow behavior, *Composites Part A* 124 (2019), 105476, <https://doi.org/10.1016/j.compositesa.2019.105476>.
- [8] F. Wittemann, *Fiber-dependent Injection Molding Simulation of Discontinuous Reinforced polymers: Doctoral Thesis, Karlsruher Institut für Technologie (KIT), Karlsruhe, Germany, 2022*.
- [9] N. Meyer, L. Schöttl, L. Bretz, A.N. Hrymak, L. Kärger, Direct Bundle Simulation approach for the compression molding process of Sheet Molding Compound, *Composites Part A* 132 (2020), 105809, <https://doi.org/10.1016/j.compositesa.2020.105809>.
- [10] N. Meyer, *Mesoscale Simulation of the Mold Filling Process of Sheet Molding Compound: Doctoral Thesis, Karlsruher Institut für Technologie (KIT), Karlsruhe, Germany, 2021*.
- [11] A.J. Favaloro, H.-C. Tseng, R.B. Pipes, A new anisotropic viscous constitutive model for composites molding simulation, *Composites Part A* 115 (2018) 112–122, <https://doi.org/10.1016/j.compositesa.2018.09.022>.
- [12] G.B. Jeffery, The motion of ellipsoidal particles immersed in a viscous fluid, *Proc. R. Soc. London* 102 (1922) 161–179.
- [13] F. Folgar, C.L. Tucker, Orientation Behavior of Fibers in Concentrated Suspensions, *J. Reinf. Plast. Compos.* 3 (1984) 98–119.
- [14] J. Wang, J.F. O'Gara, C.L. Tucker, An objective model for slow orientation kinetics in concentrated fiber suspensions: theory and rheological evidence, *J. Rheol. (N Y N Y)* 52 (2008) 1179–1200, <https://doi.org/10.1122/1.2946437>.
- [15] J.H. Phelps, C.L. Tucker, An anisotropic rotary diffusion model for fiber orientation in short- and long-fiber thermoplastics, *J. Nonnewton Fluid Mech* 156 (2009) 165–176, <https://doi.org/10.1016/j.jnnfm.2008.08.002>.
- [16] S.G. Advani, C.L. Tucker, The Use of Tensors to Describe and Predict Fiber Orientation in Short Fiber Composites, *J. Rheol. (N Y N Y)* 31 (1987) 751–784, <https://doi.org/10.1122/1.549945>.
- [17] S.G. Advani, C.L. Tucker, Closure approximations for three-dimensional structure tensors, *J. Rheol. (N Y N Y)* 34 (1990) 367–386, <https://doi.org/10.1122/1.550133>.

- [18] H. Du Chung, T.H. Kwon, Invariant-based optimal fitting closure approximation for the numerical prediction of flow-induced fiber orientation, *J. Rheol. (N Y N Y)* 46 (2002) 169–194, <https://doi.org/10.1122/1.1423312>.
- [19] J.P. Hernandez, T. Raush, A. Rios, S. Strauss, T.A. Osswald, Theoretical analysis of fiber motion and loads during flow, *Polym. Compos.* (2004) 25.
- [20] A. Durin, P. de Micheli, J. Ville, F. Inceoglu, R. Valette, B. Vergnes, A matricial approach of fibre breakage in twin-screw extrusion of glass fibres reinforced thermoplastics, *Composites Part A* 48 (2013) 47–56, <https://doi.org/10.1016/j.compositesa.2012.12.011>.
- [21] J.H. Phelps, A.I. Abd El-Rahman, V. Kunc, C.L. Tucker, A model for fiber length attrition in injection-molded long-fiber composites, *Composites, Part A* 51 (2013) 11–21, <https://doi.org/10.1016/j.compositesa.2013.04.002>.
- [22] K. Shon, D. Liu, J.L. White, Experimental Studies and Modeling of Development of Dispersion and Fiber Damage in Continuous Compounding, *Int. Polym. Proc.* 20 (2005) 322–331, <https://doi.org/10.3139/217.1894>.
- [23] F. Wittemann, L. Kärger, F. Henning, Theoretical approximation of hydrodynamic and fiber-fiber interaction forces for macroscopic simulations of polymer flow process with fiber orientation tensors, *Compos., Part C* 132 (2021), 100152, <https://doi.org/10.1016/j.jcomc.2021.100152>.
- [24] A. Bernath, Numerical Prediction of Curing and Process-Induced Distortion of Composite structures: Doctoral Thesis, Karlsruhe, Karlsruhe, Germany, 2020.
- [25] F. Wittemann, R. Maertens, A. Bernath, M. Hohberg, L. Kärger, F. Henning, Simulation of Reinforced Reactive Injection Molding with the Finite Volume Method, *J. Compos. Sci.* 2 (2018) 5, <https://doi.org/10.3390/jcs2010005>.
- [26] J. Tamil, S.H. Ore, K.Y. Gan, S.H. Ore, K.Y. Gan, Y.Y. Bo, G. Ng, P.T. Wah, N. Suthiwongsunthorn, S. Chungpaiboonpatana, Molding Flow Modeling and Experimental Study on Void Control for Flip Chip Package Panel Molding with Molded Underfill Technology, *Int. Symp. Microelectron.* 2011 (2012//2011) 673–682, <https://doi.org/10.4071/isom-2011-WP1-Paper4>.
- [27] E. Ruiz, F. Waffo, J. Owens, C. Billotte, F. Trochu, Modeling of resins cure kinetics for molding cycle optimization, in: *The 8th International Conference on Flow Processes in Composite Materials (FPCM8)*, Douai (France), 2006, pp. 221–230.
- [28] A.G. Gibson, Die entry flow of reinforced polymers, *Composites* 20 (1989) 57–64, [https://doi.org/10.1016/0010-4361\(89\)90683-6](https://doi.org/10.1016/0010-4361(89)90683-6).
- [29] S.M. Dinh, R.C. Armstrong, A Rheological Equation of State for Semiconcentrated Fiber Suspensions, *J. Rheol. (N Y N Y)* 28 (1984) 207–227, <https://doi.org/10.1122/1.549748>.
- [30] X. Fan, N. Phan-Thien, R. Zheng, A direct simulation of fibre suspensions, *J. Nonnewton. Fluid Mech.* 74 (1998) 113–135, [https://doi.org/10.1016/S0377-0257\(97\)00050-5](https://doi.org/10.1016/S0377-0257(97)00050-5).
- [31] S.B. Lindström, T. Uesaka, Simulation of the motion of flexible fibers in viscous fluid flow, *Phys. Fluids* 19 (2007), 113307, <https://doi.org/10.1063/1.2778937>.
- [32] G.K. Batchelor, *An Introduction to Fluid Dynamics*, Cambridge University Press, Cambridge, 2000.
- [33] R. Maertens, A. Hees, L. Schöttl, W. Liebig, P. Elsner, K.A. Weidenmann, Fiber shortening during injection molding of glass fiber-reinforced phenolic molding compounds: fiber length measurement method development and validation, *Polymer-Plastics Technol. Mater.* (2021) 1–14, <https://doi.org/10.1080/25740881.2020.1867170>.
- [34] J.G. Brodnyan, The Concentration Dependence of the Newtonian Viscosity of Prolate Ellipsoids, *Trans. Soc. Rheol.* 3 (1959) 61–68, <https://doi.org/10.1122/1.548843>.
- [35] K.D. Ziegel, F.R. Eirich, Isotope effect in gas transport. II. Effect of the glass transition on the size of the free volume element, *J. Polym. Sci., Polym. Phys. Ed.* 12 (1974) 1127–1135, <https://doi.org/10.1002/pol.1974.180120608>.
- [36] T. Kitano, T. Kataoka, T. Shirota, An empirical equation of the relative viscosity of polymer melts filled with various inorganic fillers, *Rheol. Acta* 20 (1981) 207–209, <https://doi.org/10.1007/BF01513064>.
- [37] R.B. Pipes, J.W.S. Hearle, A.J. Beaussart, R.K. Okine, Influence of Fiber Length on the Viscous Flow of an Oriented Fiber Assembly, *J. Compos. Mater.* 25 (1991) 1379–1390, <https://doi.org/10.1177/002199839102501008>.
- [38] S.F. Shuler, D.M. Binding, R. Byron Pipes, Rheological behavior of two- and three-phase fiber suspensions, *Polym. Compos.* 15 (1994) 427–435, <https://doi.org/10.1002/pc.750150607>.